RSC Advances

PAPER

View Article Online
View Journal | View Issue

Cite this: *RSC Adv.*, 2017, **7**, 14876

Graphene oxide/Fe_3O_4/SO_3H nanohybrid: a new adsorbent for adsorption and reduction of Cr(VI) from aqueous solutions†

Abdolhamid Alizadeh,*[ab] Gisya Abdi,[a] Mohammad Mehdi Khodaei,[a] Muthupandian Ashokkumar[c] and Jhaleh Amirian[d]

Received 6th February 2017
Accepted 26th February 2017

DOI: 10.1039/c7ra01536d

rsc.li/rsc-advances

A sulfonated magnetic graphene oxide (SMGO) hybrid was successfully synthesized *via* the nucleophilic substitution reaction and characterized. The removal of chromate by SMGO was investigated. The effects of contact time, initial pH of the solution, and initial chromate concentration on the removal efficiency were investigated. The optimal experimental conditions for enhanced chromate removal were found to be a contact time of 60 min at an initial solution pH of 3. The observed data were fitted with Lagergren pseudo-second-order kinetic model, indicating that chromate adsorption on SMGO was a chemical interaction in nature. The Langmuir model was also used to describe the adsorption processes and the adsorption capacity was found to be 222.22 mg g^{-1}. Thermodynamic studies ($\Delta G < 0$, $\Delta H > 0$, $\Delta S > 0$) revealed that the adsorption process was exothermic and spontaneous. SMGO has potential to be applied several times after desorption in wastewater treatment.

1. Introduction

Heavy metal ion contamination in wastewater has become a severe environmental issue.[1,2] Among these heavy metal ions, chromium ions could cause severe health problems for both animals and human beings.[3–5] Chromium ions are present in the environment in several different forms. The most common oxidation forms are hexavalent (Cr(IV)) and trivalent (Cr(III)). While, Cr(III) is generally nontoxic, Cr(VI) is one of the most toxic heavy metal ions.[6,7] Therefore, the removal of Cr(VI) from wastewater is a hot research topic in environmental science and technology areas. The removal of Cr(VI) has been extensively investigated by various methods that include chemical precipitation, ion exchange, neutralization, membrane separation, flocculation, bio-treatment, ultrafiltration and adsorption strategies.[8,9] Adsorption is an easy, economic and promising method for sewage purification, which has the characteristics of high selectivity and ease of operation.[10,11] The adsorbent plays a key role in the adsorption process. Therefore, the design and synthesis of adsorbents with excellent performance are important in adsorption research.[12]

Graphene oxide (GO) and reduced graphene oxide (RGO) are flexible lamellar materials with large specific surface areas and aromatic sp^2 domains. GO possesses a wide range of functional groups such as epoxy (C–O–C), hydroxyl (OH), and carboxyl (COOH) groups on its backbone and edges, which render strong hydrophilic properties and excellent adsorption capacity for heavy metal pollutants.[13,14] However, most of these materials are used as nanosized sorbent particles and are difficult to collect from water following treatment, which restricts their practical application.[15] The incorporation of magnetic particles on the surface of GO can combine the high adsorption capacity of GO and the separation convenience of magnetic materials.[16,17] In order to increase the adsorption ability of these materials, a great number of GO derivatives have been synthesized by grafting new functional groups onto GO backbone.[18]

In this work, GO/Fe_3O_4/SO_3H hybrid was prepared and its use as an adsorbent for Cr(IV) evaluated. The hybrid material was also characterized by a number of analytical techniques.

2. Materials and methods

2.1 Materials

Graphite powder, chlorosulphonic acid, sodium hydroxide, potassium dichromate, potassium permanganate, ferric chloride hexahydrate ($FeCl_3 \cdot 6H_2O$) and ferrous chloride tetrahydrate ($FeCl_2 \cdot 4H_2O$) were purchased from Sigma Aldrich. Chlorosulphonic acid, hydrochloridric acid, orthophosphoric

[a]*Department of Organic Chemistry, Faculty of Chemistry, Razi University, Kermanshah, 6714967346, Iran. E-mail: ahalizadeh2@hotmail.com; ahalizadeh2@razi.ac.ir; Fax: +98 833 427 4559; Tel: +98 833 427 4559*

[b]*Nanoscience & Nanotechnology Research Center (NNRC), Razi University, Kermanshah, Iran*

[c]*School of Chemistry, University of Melbourne, VIC 3010, Australia*

[d]*Department of Regenerative Medicine, College of Medicine, Soonchunhyang University, 366-1, Sangyong-dong, Cheonan-City, Chung Cheong Nam-Do 330-090, Republic of Korea*

† Electronic supplementary information (ESI) available. See DOI: 10.1039/c7ra01536d

acid, ammonia and ethanol were procured from Merck. All other reagents used in this study were analytical grade, and distilled or double distilled water was used in the preparation of all solutions.

2.2 Characterization

X-ray photoelectron spectroscopy (XPS) spectra were obtained by using the ESCALAB 250 X-ray Photoelectron Spectroscopy/ESCA equipment. X-ray diffraction (XRD) spectra were recorded on D/MAX-250, Rigaku, Tokyo, Japan using 40 kV with Cu Kα irradiation ($\lambda = 1.541$ Å). Fourier transform infrared (Bruker FTIR) spectra were recorded in KBr pellets in the range of 400–4000 cm^{-1}. Scanning electron microscopy (SEM) images of the product were taken using a JSM-6701F microscope (JEOL, Japan) equipped for EDS. A small part of scaffold was placed on the SEM sample holder and sputter coated with platinum. An accelerating voltage of 10 kV was used. Transmission electron microscopy (TEM) was performed on JEOL JEM-1010n. The magnetic measurements were carried out in a vibrating sample magnetometer (VSM, BHV-55, Riken, Japan) at room temperature. Measurements of Raman spectra were carried out using a Senterra Raman Scope system with a 532 nm wavelength incident laser light and power 20 mW. Brunauer–Emmett–Teller (BET) specific surface area and pore volume were measured by nitrogen adsorption using Micromeritics Tristar 3020. The pore size distribution for each sample was calculated using non-local density functional theory (NLDFT), from the desorption branch of the isotherms. Thermogravimetric analysis (TGA) was carried out using a Q5000IR (TA instruments) under nitrogen flow (100 mL min^{-1}) with ramp rate of 10 °C min^{-1}. UV-visible spectra were recorded by Perkin Elmer Lambda 25 spectrometer.

2.3 Methods

2.3.1 Synthesis of graphene oxide. Graphene oxide was synthesized by oxidation of graphite using the modified Hummer's method.[19] To a mixture of 6 g $KMnO_4$ and 1 g graphite, 120 mL of concentrated sulfuric acid and 15 mL of orthophosphoric acid were poured. It was heated to 50 °C and stirred for 24 h. The resulting mixture was added to ice (150 mL) with 6 mL of H_2O_2 (30%), turning the color of the solution from dark brown to yellow. The solution was centrifuged and separated solid product (dark brown GO) was washed two times with water, 30% HCl and ethanol (ESI Fig. S1†).

2.3.2 Synthesis of GO/Fe_3O_4/SO_3H hybrid (SMGO). The GO/Fe_3O_4 hybrid was synthesized from GO suspension (0.2 g) in 250 mL solution of 1.86 g $FeCl_3 \cdot 6H_2O$ and 0.6 g $FeCl_2 \cdot 4H_2O$ at room temperature under N_2. The mixed aqueous solution of $FeCl_3$ and $FeCl_2$ was added slowly to the GO suspension, and the ammonia solution was added quickly to precipitate Fe^{2+}/Fe^{3+} ions for synthesis of magnetite (Fe_3O_4) particles. Ammonia solution (30%) was added to adjust the pH to 10. After rapidly stirred for 2 hours, the dark black solution was filtered and washed with deionized water/ethanol and dried in a vacuum at 70 °C to obtain GO/Fe_3O_4.

GO/Fe_3O_4/SO_3H hybrid was synthesized by adding dropwise chlorosulfonic acid (20 mmol, 1.2 cm^3) to 0.2 g GO/Fe_3O_4 suspension in 20 mL dichloromethane (CH_2Cl_2) with constant stirring in an ice bath for 2 h. The resulted paste was washed repeatedly until pH was about 7.0. Then, the obtained product was collected by the aid of a permanent magnet and dried in a vacuum oven at 50 °C to obtain GO/Fe_3O_4/SO_3H.

2.3.3 Determination of the content of acid groups on SMGO hybrid. The content of acid groups of SMGO was determined by acid–base titration. SMGO hybrid (0.25 g) was dissolved in NaOH (15 mL, 0.05 M) and purged with argon for at least 60 min. After 1 hour stirring, the suspensions were slowly back-titrated with 0.05 M HCl solution to reach the neutral point (pH 7). The amount of acid groups was found to be 0.36 mmol for the SMGO hybrid sample. From elemental analysis (22.5% weight S and 15.9% weight C), the amounts of SO_3H and COOH were estimated to be 0.21 mmol 0.15 mmol, respectively.

2.3.4 Adsorption experiments. The adsorption experiments were performed using a batch equilibration technique at 25.0 °C. Simulated wastewater with different Cr(VI) concentrations (50, 80, 100, 120, 150, 180 and 200 mg L^{-1}) were prepared by dilution of the stock $K_2Cr_2O_7$ standard solution with deionized water. Known masses of sorbent (GO/Fe_3O_4/SO_3H) were mixed with 40 mL of above Cr(VI) solution in centrifuge tubes. The centrifuge tubes were shaken in a thermostatic water bath shaker. After the adsorption processes, the solid and liquid phases were separated by a permanent magnet (Fig. 6 right inset). The instantaneous Cr(VI) concentrations in liquid phase was immediately analyzed by UV-visible spectrometry[20] at 350 nm and C_t and q_t were calculated. The adsorption behavior of the SMGO hybrid was investigated at different pH values of Cr(VI) solution. The solution pH was adjusted using 0.1 M NaOH or 0.1 M HCl as required. For kinetic studies, the pH was fixed at a value corresponding to maximum adsorption and 0.5 g L^{-1} of SMGO hybrid was used. The initial concentration of the Cr(VI) was fixed at 100 mg L^{-1} and adsorption time was varied from 5 to 240 min. The adsorption isotherms were tested to validate Cr(VI) uptake behavior of the SMGO. Adsorption behavior was studied at 298, 313, and 333 K to find the thermodynamics of the adsorption process.

3. Results and discussion

3.1 Synthesis and characterization of GO/Fe_3O_4/SO_3H hybrid (SMGO)

The interaction between GO, Fe_3O_4 or GO/Fe_3O_4 and chlorosulphonic acid has three possibilities: hydrogen bonding, electrostatic interaction and nucleophilic substitution reaction. As depicted in Scheme 1, the nucleophilic reaction between surface hydroxyl or epoxy groups with chloro group is presumably the dominant possibility for this attachment. These may lead to the covalent attachment of –SO_3H moiety onto the surface of GO, Fe_3O_4 or GO/Fe_3O_4 (Scheme 1). In order to identify the interaction between GO/Fe_3O_4 hybrid and chlorosulphonic acid, the obtained GO/Fe_3O_4/SO_3H was characterized by FTIR. Fig. 1 depicts the FTIR signals of GO, GO/Fe_3O_4,

and GO/Fe_3O_4/SO_3H hybrid. Fig. 1A reveals the characteristic absorption peaks for GO at 1728, 1629, 1422, 1052 and 1225 cm^{-1}, which can be attributed to C=O stretching, C=C in-plane stretching vibration, adsorbed water molecules, O–H deformation, alkoxy C–O stretching, and epoxy C–O stretching vibration, respectively.[21] All these results clearly indicate the formation of graphene oxide and presence of oxygenated functionalities on a graphene skeleton, which we have used for the growth of magnetic nanoparticles. FTIR spectrum of magnetic graphene oxide (MGO) is shown in Fig. 1B. The peak at 1728 cm^{-1} corresponding to C=O of carboxyl group on the GO shifts to 1638 cm^{-1}, may be due to the formation of $-COO^-$ after coating with Fe_3O_4. FTIR spectrum show two broad peaks at 1587 and 1084 cm^{-1} which correspond to the aromatic C=C stretch and C–O stretch, respectively. The transmittance band around 583 cm^{-1} is attributed to Fe–O. The FTIR spectra of SMGO hybrid (Fig. 1C) shows a peak at 1729 cm^{-1} corresponding to the stretching vibration of carbonyl (C=O) groups on the GO, and the strong broad band centered at approximately 3437 cm^{-1} was assigned to the O–H stretching modes of the hydroxyl groups on SMGO hybrid.[22]

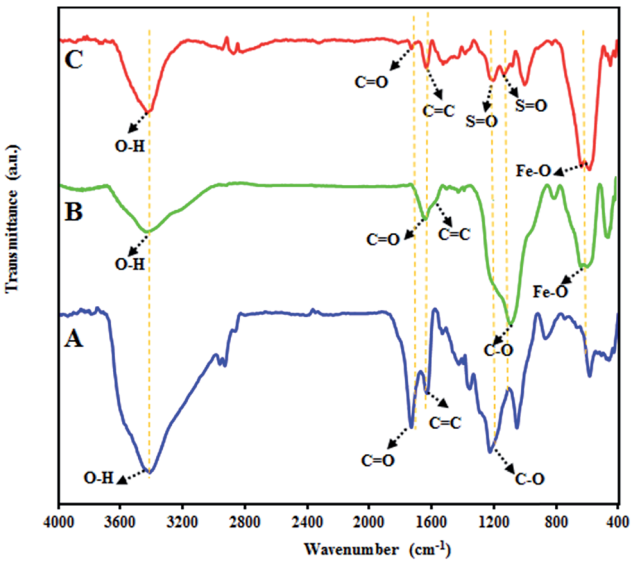

Fig. 1 FTIR spectra of (A) GO, (B) MGO, and (C) SMGO hybrid.

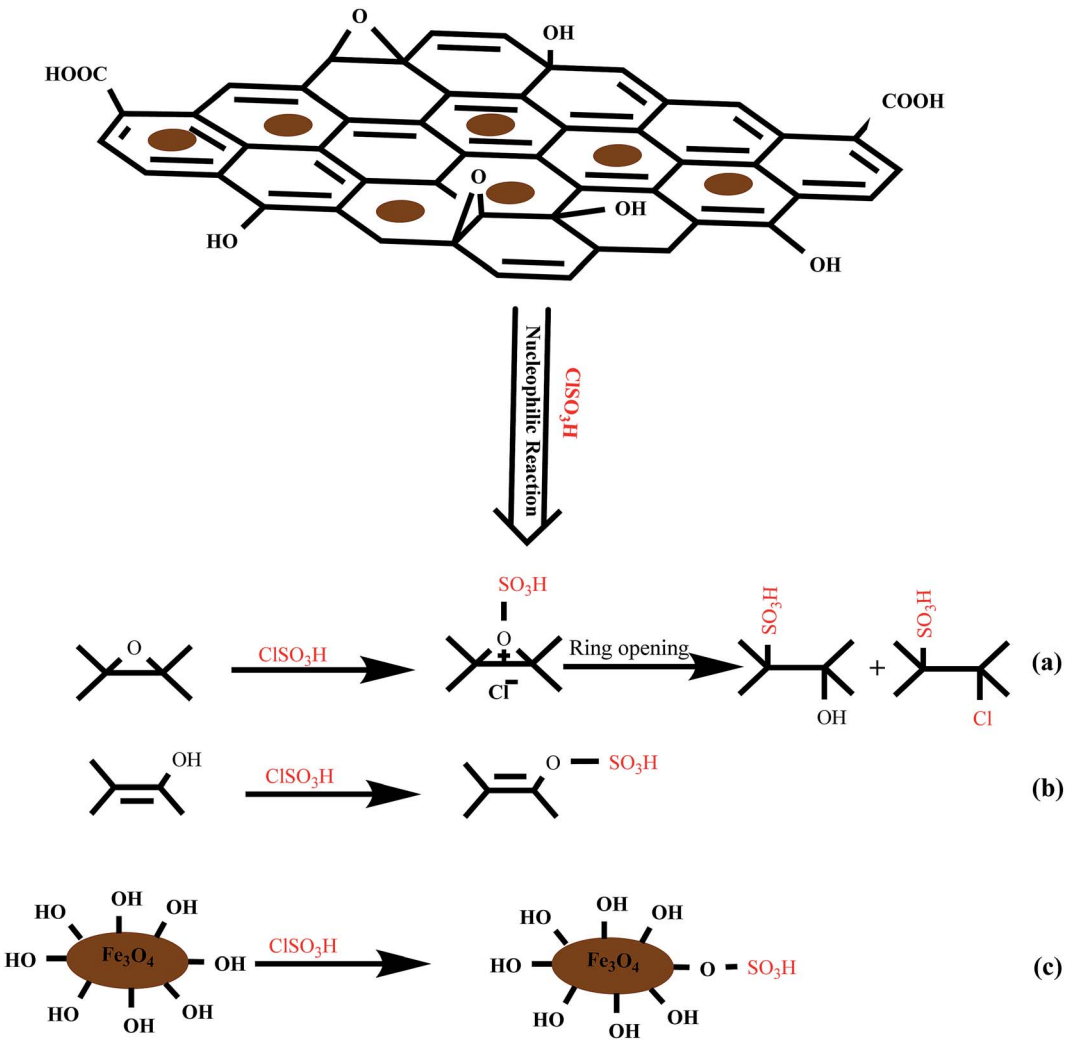

Scheme 1 Proposed nucleophilic substitution reactions for modification of magnetic graphene oxide by chlorosulphonic acid.

The peak at 1634 cm^{-1} corresponds to aromatic stretch C=C. The peaks at 1199 and 1129 cm^{-1} confirmed the presence of S=O group.[23,24] The peak at 574 cm^{-1} is a characteristic peak corresponding to the stretching vibration of Fe–O.[25]

Fig. 2 shows XRD patterns of GO and GO/Fe_3O_4/SO_3H. The XRD pattern of GO showing a sharp diffraction peak at scattering angle $2\theta = 10°$ corresponding to (001) plane of GO, giving the interlayer separation to be ~8.83 Å. The increased *d*-spacing of GO sheets is due to the presence of abundant oxygen-containing functional groups on both sides of the grapheme sheet causing an atomic-scale roughness on the grapheme sheet. The XRD patterns of SMGO hybrids (Fig. 2B) show diffraction peaks indexed to (111), (220), (311), (400), (422), (511), and (440) planes appearing at $2\theta = 17.53$, 30.40°, 35.67°, 43.33°, 53.24°, 57.34°, and 62.85°, respectively, which are consistent with the standard XRD data for the cubic phase Fe_3O_4 with a face-centered cubic (fcc) structure.[26] The broad diffraction peaks are indications of the nanoparticles with very small size. The broad peak which appears at 22.0 attributed to reduced graphene oxide (RGO).[22] X-ray powder diffraction patterns of GO/Fe_3O_4/SO_3H were recorded using CuK_α radiation ($\lambda = 1.542$ Å).

The X-ray photoelectron spectroscopy (XPS) was used to investigate the chemical changes brought by magnetite nanoparticles. ESI Fig. S2A† shows the wide scan X-ray photoemission spectroscopy (XPS) of SMGO hybrid. The XPS spectra of the SMGO shows photoelectron lines at a binding energy of about 167.6, 284.5, 530, 711 eV attributed to S2p, C1s, O1s, and Fe2p, respectively (ESI Fig. S2†). The C1s XPS spectrum of GO with peak-fitting curves is presented in Fig. 3A. The peaks at 284.9, 286.2, 288.3, and 289.3 eV were assigned to carbon atoms in the C–C bond (sp^2), C–O, C=O and O–C=O, respectively.

This result suggested that GO contained large numbers of functional groups on its surface. Compared with GO, the intensity of the C–O and C=O peaks in the SMGO composite shown in Fig. 3B is dramatically decreased, indicating effective deoxygenation of GO after reduction by magnetic nanoparticles. It is notable that the peaks of O1s in SMGO composite spectra shifted to lower binding energy and broadened, which is characteristic of the O1s in Fe_3O_4 lattice (ESI Fig. S2C†).

Raman spectroscopy is widely used to characterize crystal structure, disorder and defects in graphene-based materials. Fig. S-3 in ESI† presents the Raman spectra (532 nm excitation) of GO (A) and SMGO composite (B). The D-band (1373 cm^{-1}) and G-band (1594 cm^{-1}) are two predominate peaks[27] for GO. The G-band for GO due to the presence of isolated double bonds appeared at frequencies higher than that of the G-band of the graphite (1580 cm^{-1}).[28] The G-band of SMGO occurred at 1577 cm^{-1}, and peak at 1363 cm^{-1} was attributed to D-band. The intensity ratio of D band to G band ($r = I_D/I_G$) is usually used as a measure of the disorder.[29] The intensity ratio of D band to G band ($r = I_D/I_G$) of SMGO (1.27) increased notably, indicating that the reduction process altered the structure of GO (0.89) with a high quantity of structural defects.

Surface area measurement of the SMGO *via* the nitrogen gas absorption–desorption isotherm yielded a Brunauer, Emmett and Teller (BET) surface area of 184.17 $m^2\ g^{-1}$. The pore size distribution of samples could be calculated by Barrett–Joyner–Halenda (BJH) method (ESI Fig. S4†). The SMGO exhibited average pore size centralizing at 4.19 nm (ESI Fig. S5†).

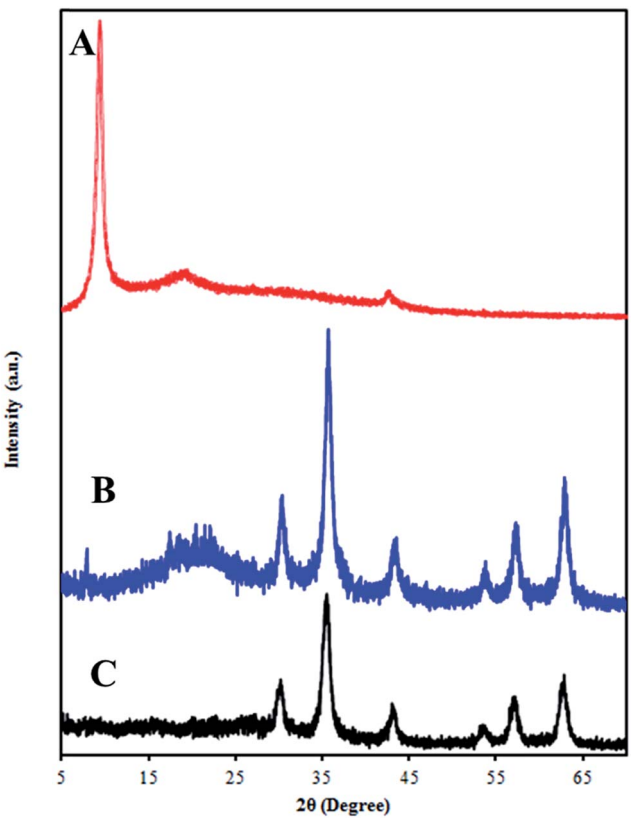

Fig. 2 XRD patterns of GO (A), SMGO (B) and (C) Fe_3O_4. The patterns of SMGO hybrids show diffraction peaks indexed to (220), (311), (400), (422), (511), and (440) planes appearing at $2\theta = 30.40°$, 35.67°, 43.33°, 53.24°, 57.34°, and 62.85°, respectively. These matched the characteristic peaks for Fe_3O_4 in the standard PDF card in the X-ray diffraction atlas (JCPDS card 19-0629) issued by the International Powder Union.

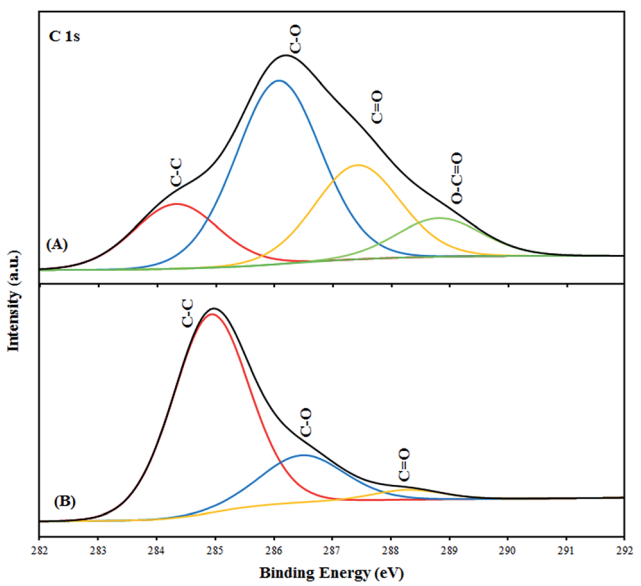

Fig. 3 X-ray photoelectron spectroscopy (XPS) spectra: C1s spectra of GO (A), of SMGO (B).

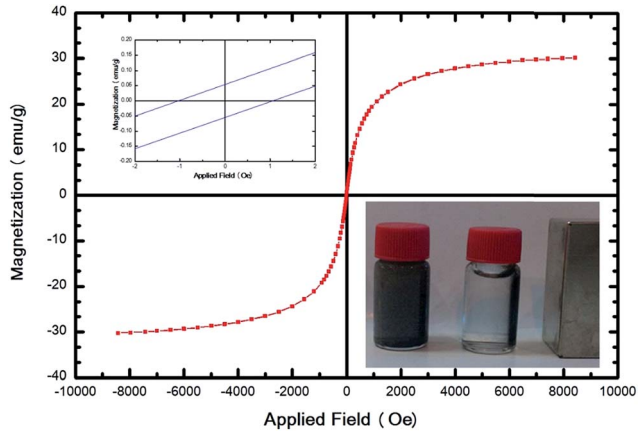

Fig. 4 Hysteresis loop of the SMGO hybrid at room temperature. The top inset: the magnified field from −2 to 2 Oe. The bottom inset: aqueous solution of SMGO (left), separated particles of SMGO by a magnet (right).

Thermogravimetric analysis (TGA) is a useful tool to determine the composition of the samples. Figure displays the TGA thermograms of GO and SMGO composite (at a heating rate of 10 °C min^{-1} and under a nitrogen atmosphere). The initial weight loss of GO below 120 °C is ascribed to the elimination of adsorbed water and the weight loss from 120 °C to ~300 °C is ascribed to decomposition and evaporation of oxygen-containing functional groups (ESI Fig. S6†). The curve for the SMGO composite shows the weight loss before 200 °C (w_t loss 8%) and another ~375 (w_t loss 7%). The nanocomposite shows far greater stability up to 800 °C.

The magnetic property of SMGO was characterized by a vibrating sample magnetometer (VSM) and Fig. 4 shows the typical room temperature magnetization curve of SMGO. The saturation magnetization (M_s) of the GO/Fe_3O_4/SO_3H hybrid is 26 emu g^{-1} (magnetic field ± 10 kOe) (Fig. 4), indicating the high magnetic property. The left inset in Fig. 4 is the magnification of hysteresis loop of GO/Fe_3O_4/SO_3H. The right inset of Fig. 4 shows that SMGO hybrid is attracted by an external magnet, and the clear solution can be easily removed by pipette or decanting. It has been reported that the Fe_3O_4 nanoparticles with a high value of coercivity (H_c) could be called ferromagnetic at room temperature, whereas those with a low value (lower than 20 Oe) could be called superparamagnetic.[30] Our results showed that the H_c of catalysts is 1.05 Oe and the M_r (remnant magnetization) is ~0.055 emu g^{-1}.

The scanning electron microscopy (SEM) and transmission electron microscopy (TEM) images of the GO and SMGO hybrids are shown in Fig. 5. The presence of magnetite in SMGO hybrid and folding nature of graphene oxide sheets can be seen throughout the morphology (Fig. 5B). The TEM images are shown in Fig. 5C and D, and the crumpled graphene oxide sheets and the presence of magnetite nanoparticles suggest that GO/Fe_3O_4 hybrids are formed. The TEM image (Fig. 4D) shows that the GO film is transparent and Fe_3O_4 nanoparticles are dispersed on the surface. The quantitative elemental analyses of

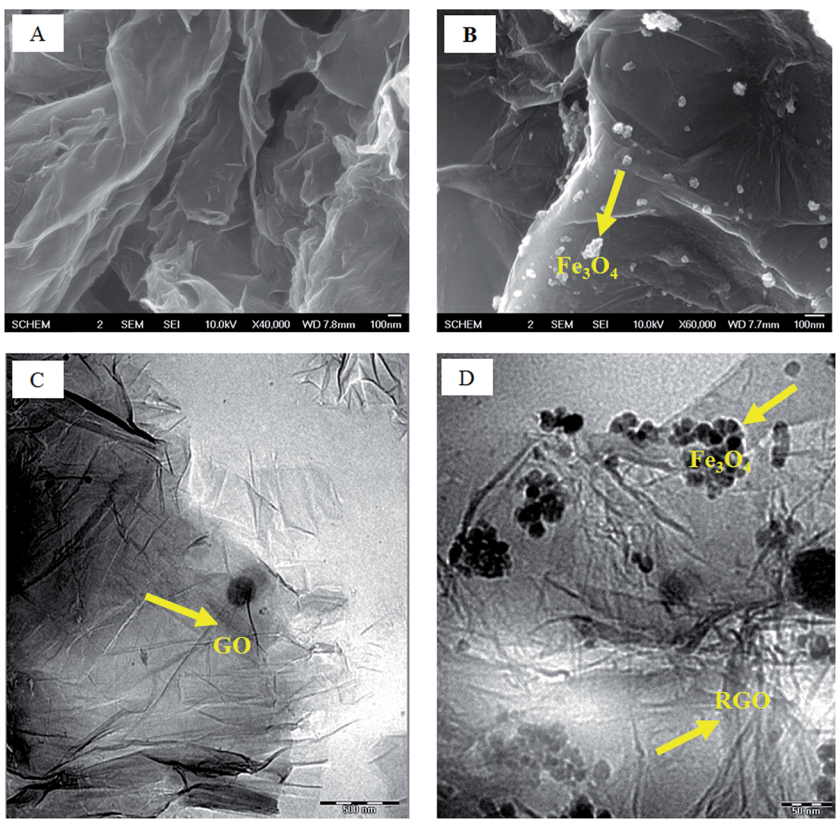

Fig. 5 SEM and TEM images of GO (A and C), SMGO hybrid (B and D).

Table 1 Quantitative EDS analyses of the element proportion in GO, MGO, and SMGO hybrids

	Weight%		
Element	GO	MGO	SMGO
C K	47.18	38.24	15.92
O K	52.82	24.44	43.36
N K	—	2.20	—
S K	—	—	22.47
Fe L	—	35.13	18.25
Totals	100	100	100

the samples obtained by EDS (ESI Fig. S7†), results are shown in Table 1.

3.2 Adsorption study

To evaluate the performance of surface-modified GO nanosheets in Cr(VI) removal from aqueous solution, we set four parallel control experiments to make a comparison on the performance of GO, GO–SO_3H, GO/Fe_3O_4 and GO/Fe_3O_4/SO_3H as adsorbent (Table 2). GO with several hydrophilic functional groups on its backbone and edges has excellent adsorption capacity for heavy metal pollutant. However, as GO nanosheets are nanosized adsorbent, their collection is very difficult or impossible from water following treatment and this restricts their practical application. In addition, grafting new functional groups onto GO backbone presumably lead to increase in the adsorption ability of GO sheets. In a simple treatment of GO with $ClSO_3H$, another adsorbent (GO–SO_3H) were prepared and employed as adsorbent. It was found that GO and GO–SO_3H were completely dispersed in water (ESI Fig. S8†). At the end of adsorption test, their high dispersity in water made their separation very difficult from water solution even with the help of high speed centrifuging process (Table 2). Even though their high adsorption capacity is useful to remove pollutant, due to the difficulty of their separation they can became contamination. The incorporation of magnetic particles on the surface of GO can combine the high adsorption capacity of GO and the separation convenience of magnetic material. So, the adsorbent GO/Fe_3O_4 was prepared and employed as an easily separable adsorbent in Cr(VI) removal. But since the preparation of this composite take places in the presence of 30% NH_3 (~pH 10), its surface charge was negative and GO/Fe_3O_4 was not suitable adsorbent for removing of $HCrO_4^-$ anion. Combining GO, Fe_3O_4 and SO_3H led to a hybrid material showing excellent adsorption capacity for heavy metal pollutant with feasibility in final separation. Based on our further investigations, GO/Fe_3O_4/SO_3H (SMGO) adsorbent showed excellent performance in Cr(VI) removal from water.

Table 2 Comparison on the performance of GO, GO–SO_3H, GO/Fe_3O_4 and GO/Fe_3O_4/SO_3H as adsorbent in Cr(VI) removal

		Separation with	
Adsorbent	Dispersity in water	Centrifuge	External magnet
GO	✓	Trace	—
GO/SO_3H	✓	Trace	—
GO/Fe_3O_4	✗	—	✓
GO/Fe_3O_4/SO_3H	✗	—	✓

3.2.1 pH effect of the solution. The pH of the solution is a key factor which affects the charge of the adsorbent surface and control the adsorption process. The adsorption data of SMGO in various pH is shown in Fig. 6. The initial pH values of the solution were adjusted to 2.0, 3.0, 4.0, 5.0, 8.0 and 10.0.

The concentration of SMGO was 0.5 g L^{-1}, and the initial Cr(VI) concentration was 100 mg L^{-1}. The amount of the ionic metal adsorbed on adsorbent is calculated using the relation $q_t = (C_0 - C_t)/m)V$. Here, q_t (mg g^{-1}) is the amount of metal ions adsorbed by the adsorbent at t time condition, C_0 is the initial metal ion concentration, C_e is the metal ion concentration at equilibrium, V is the volume of the initial chromate solutions, and m is the mass of the adsorbent. The maximum adsorption occurs at pH = 3. Upon addition of SMGO to the solution, there was a slight change in pH; the initial pH and final pH were 3 and 2.86 values, respectively. This might be due to the acidic nature of poly sulphonated composite.

3.2.2 Adsorption kinetics. After finding the optimum pH, the adsorption of Cr(VI) from aqueous solution on GO/Fe_3O_4/SO_3H as a function of contact time was investigated, results are shown in Fig. 7. The adsorption of Cr(VI) increase rapidly during the first 60 min, then remains constant with increasing of contact time. According to this result, 60 min was selected as the shaking time to ensure the full equilibrium in the following experiments.

In the adsorption kinetic studies Lagergren pseudo-first-order model and pseudo-second-order model are often used to reveal the mechanism of adsorption process, which can be expressed as follows:

$$\ln(q_e - q_t) = -k_1 t + \ln q_e \quad (1)$$

$$\frac{t}{q_t} = \frac{1}{k_2 q_e^2} + \frac{t}{q_e} \quad (2)$$

Where q_t (in mg g^{-1}) are the equilibrated adsorption capacities, k_1 (in min^{-1}) and k_2 (in g mg^{-1} min^{-1}) are rate

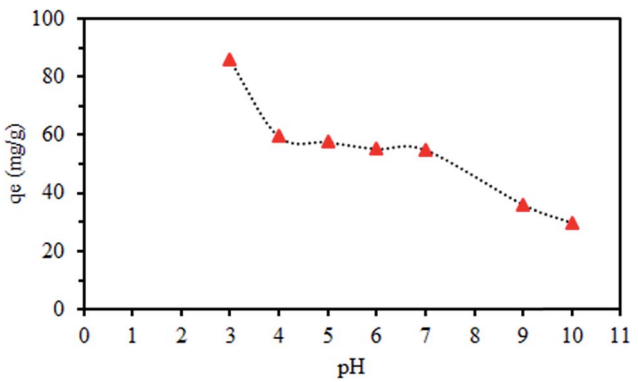

Fig. 6 Influence of initial pH of solution on the adsorption capacity of Cr(VI). Mass of SMGO hybrids = 0.5 g L^{-1}, initial concentration of Cr(VI) = 100 mg L^{-1}, contact time = 60 min, volume of Cr(VI) solution = 40 mL, temperature = 20 °C.

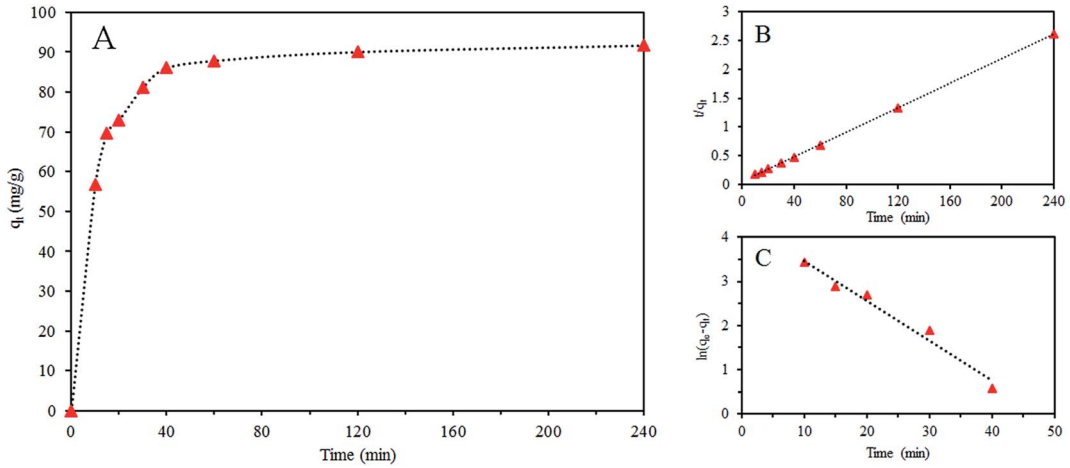

Fig. 7 Effect of time on the adsorption capacity (A), the fitting results of the experimental adsorption kinetic data in terms of pseudo-first-order (B) and pseudo-second-order (C) models (pH: 3, Cr(VI) concentration: 100 mg g^{-1}, volume of Cr(VI) solution: 40 mL, adsorbent dose 0.5 g L^{-1}, and temperature: 298 K).

constants of the pseudo-first-order and pseudo-second-order kinetic models, and t (min) is contact time.

As shown in Fig. 7 and Table 3, we found that the coefficient of determination (R^2) of pseudo-second-order model for Cr(VI) is 0.999, which is higher than the value obtained by the pseudo-first-order model, indicating adsorption of Cr(VI) on GO/Fe_3O_4/SO_3H can be described by the Lagergren pseudo-second-order kinetic model and its adsorption rate is determined by the chemical adsorption.

3.2.3 Adsorption isotherm studies. It is a vital step to find out the most suitable isotherm model to describe the adsorption process by fitting experimental data to different models. As the most frequently used isotherm models, the Langmuir and Freundlich models are used to analyze the experimental data of Cr(VI) adsorption in the present study, and the linear form of the Langmuir model could be expressed as follows:

$$\frac{C_e}{q_e} = \frac{1}{(K_L q_m)} + \frac{C_e}{q_m} \quad (3)$$

The linear form of Freundlich model could be expressed as follows (eqn (4)):

$$\ln q_e = \ln K_F + \frac{1}{n} \ln C_e \quad (4)$$

Where C_e (in mg L^{-1}) is the concentration of equilibrium, q_e (in mg g^{-1}) is the equilibrated adsorption capacity, K_L (in L mg^{-1}) and q_m (in mg g^{-1}) are Langmuir parameters relevant to energy and capacity of adsorption, and n and K_F (in mg^{1-n} L^n g^{-1}) are Freundlich parameters to the intensity and capacity of adsorption.

To judge whether the adsorption process is favorable or not, a dimensionless constant referred to as separation factor or equilibrium parameter R_L is calculated using following eqn (5):[31]

$$R_L = \frac{1}{1 + K_L C_0} \quad (5)$$

Where K_L (L mg^{-1}) is the Langmuir constant and C_0 (mg L^{-1}) is the initial concentration of chromate solution. The R_L value indicates adsorption process is irreversible when R_L is 0; favorable when R_L is between 0 and 1; linear when R_L is 1; and unfavorable when R_L is greater than 1.

Isotherms of Cr(VI) adsorption on SMGO hybrid are illustrated in Fig. 8. Fitting adsorption equilibrium data to these two models, isotherm parameters were obtained and shown in Table 4. It is obvious that an increase in the initial metal ion concentration leads to a decrease in adsorption percentage but contributes to the increase of adsorption capacities for Cr(VI), which suggests that SMGO hybrid has great potential in the treatment of wastewater contaminated with high concentration of Cr(VI).

The related parameters of the two models are tabulated in Table 4. Moreover, R^2 of Langmuir model is more precise in evaluating adsorption equilibrium, the fact that the adsorption data of Cr(VI) is in accordance with the Langmuir model suggests that monolayer coverage of chromium on SMGO is the main adsorption mechanism and the surface of SMGO

Table 3 The first-order and second-order kinetics constants for adsorption of Cr(VI) on the SMGO

Experimental	First-order kinetic			Second-order kinetic		
$q_{e,exp}$ (mg g^{-1})	k_1	$q_{e,cal}$ (mg g^{-1})	R^2	k_2	$q_{e,cal}$ (mg g^{-1})	R^2
87.82	0.0906	80.16	0.975	0.0021	93.45	0.999

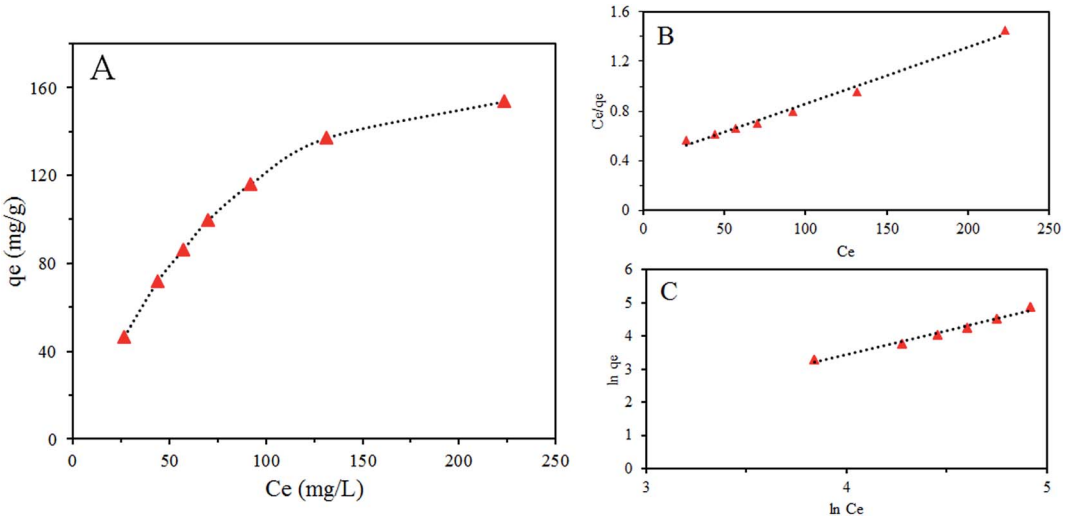

Fig. 8 (A) Equilibrium isotherm for adsorption of Cr(VI). The fitting results of the experimental adsorption isotherm data in terms of Langmuir (B) and Freundlich (C) models (pH: 3, Cr(VI) concentration: 100 mg g^{-1}, volume of Cr(VI) solution: 40 mL, adsorbent dose 0.5 g L^{-1}, and temperature: 298 K).

Table 4 Comparison of fitting results by Langmuir and Freundlich models for Cr(VI) adsorption on SMGO

Langmuir model				Freundlich model		
q_m	K_L	R^2	R_L	K_F	n	R^2
222.22	0.0111	0.989	$0.3 < R_L < 0.64$	0.0928	0.69	0.983

hybrid is homogenous. The calculated value of R_L is in the range of 0.3–0.64, confirming that the adsorption processes is favorable.

The maximum adsorption capacity of SMGO hybrids, q_m obtained from the slope were found to be 222.22 mg g^{-1}. To compare the potential capacity of SMGO with those of other sorbents reported in the literature, we used q_m, a Langmuir parameter that has been used in most of the earlier investigations. Although a direct comparison of SMGO with other sorbents is difficult due to the different experimental conditions applied, Table 5 gives a simple comparison of the adsorption ability of the adsorption ability of different adsorption materials with SMGO. We engineered the surface of magnetic graphene oxide by SO_3H groups for adsorption of anionic pollutants. Chromate is one sample which can exist in different forms in media, as we explained in paper, generally Cr(VI) species may be represented in several forms in solution as a function of pH such as H_2CrO_4 (<1.0), $HCrO_4^-$ and $Cr_2O_7^{2-}$ (1.0–6.0), and CrO_4^{2-} (>6.0), which make its adsorption complex but with control of pH and engineering the surface of adsorbent, it is possible to overcome its multi-appearance and increase its adsorption amount. Higher adsorption capacity of present work compared to other reported adsorbents in the literatures is noteworthy. Moreover the magnetic separation convenience make SMGO an attractive sorbent for the removal of chromium.

3.3 Mechanisms of adsorption

Generally, the Cr(VI) species may be represented in several forms in solution as a function of pH such as H_2CrO_4 (<1.0), $HCrO_4^-$ and $Cr_2O_7^{2-}$ (1.0–6.0), and CrO_4^{2-} (>6.0).[39,40] So the pH is one of the most important factors affecting adsorbent, sorbate,

Table 5 Adsorption performance of SMGO towards Cr(VI) compared with other literature adsorbents

Adsorbent	Concentration of absorbent (g L^{-1})	pH	Contact time (min)	Adsorption capacity (mg g^{-1})	Ref.
Layered zinc hydroxide nitrate	1.5	8	120	194.3	32
MCM-49/MCM-41 composite	10	6	80	4.1	33
Amine-based-surfactant-modified clinoptilite	14	4	120	6.72	34
Superporous magnetic cationic cryogels	0.15	7	180	65.5	35
Magnetic ionic liquid/chitosan/graphene oxide	1.0	3	40	145.35	36
HDTMA-zeolite	25	3	240	8.83	6
Banana skin	5.0	2	30	249.6	37
Mesoporous iron–zirconium	1.0	5	600	59.9	38
Poly(catechol-diethylenetriamine-*p*-phenylenediamine)	0.5	3	48 (h)	200	2
SMGO	**0.5**	**3**	**60**	**222.22**	**This work**

and adsorption properties. At lower pH values, the hydroxyl, carboxyl and sulfonate groups on the surface of SMGO hybrids with the aid of protons in aqueous phase become positively charged due to strong protonation. The electrostatic interaction between the positively charged surface and the negatively charged $HCrO_4^-$, $Cr_2O_7^{2-}$ in the interlayer region, will enhance the Cr(VI) adsorption. The more positive the surface charge of SMGO, the more the removal of Cr(VI) from aqueous phase. Thus, higher amount of Cr(VI) will be absorbed by SMGO hybrid in the lower pH solution. To investigate the accuracy of this assumption, after adsorption process, the solution was removed and the adsorbent copiously washed with deionized water. Then, a NaOH solution (pH = 10) was added to the adsorbent and agitated for a while. Later on, the adsorbent was separated by an external magnet and a UV-Vis spectrum of the remained solution (Fig. 9C) was obtained. In this spectrum, the characteristic absorbance peak of CrO_4^{2-} which is the most stable form of Cr(VI) at pH = 10 was easily detectable at λ_{max} = 370 nm. This observation proved the fact that OH^- at pH = 10 can replace the sites of adsorbed $HCrO_4^-$ on solid phase at pH ~3 (Fig. 9B) and release them to aqueous solution in the form of CrO_4^{2-} (Fig. 10).

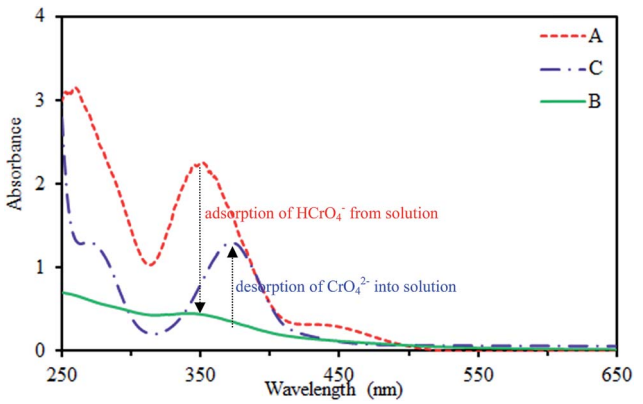

Fig. 9 UV-Vis absorption spectra of the (A) initial solution of Cr(VI) (200 mg L^{-1}) at pH = 3, (B) adsorption process at T = 318 K, and contact time = 60 min (C) desorption process at pH = 10, T = 298 K, and contact time = 60 min.

Also, the low pH of media is an appropriate factor for promotion of redox reactions in aqueous and solid phases, because protons participate in these reactions.[37,40] Hydroxyl groups and π electrons on graphene oxide sheets could act as electron-donor groups. Therefore, Cr(III) ions can be produced in aqueous and solid phases. To investigate the formation of Cr(III) in aqueous media, during the adsorption time, we considered the UV-visible spectra of solution and no absorption peak was found at wavelengths >560 nm (Fig. 9B).[41] This suggests that if the Cr(III) ions are formed based on the aforementioned possibility, they are only present on the surface of hybrid material and not freely in the solution. Due to the cationic nature of Cr(III) ion, it can be easily immobilized onto the surface of composite with the help of several groups such as OH, SO_3H and COOH. These groups all contain oxygen as donor atom and can form complex structure. This conclusion is supported by the X-ray photoelectron spectroscopy (XPS) spectra of the obtained SMGO composites after adsorption process. To prove the presence of Cr(III) on the surface of SMGO hybrid, the XPS analysis of the SMGO hybrid after adsorption was investigated. In the XPS spectrum of SMGO, the peaks of $Cr2p_{1/2}$ at 584 eV and $Cr2p_{3/2}$ at 575 eV, proved the presence of Cr(III) in the bottom layers of SMGO hybrid (ESI, Fig. S2A†).

According to aforementioned results, we proposed a plausible Cr(VI) removal mechanism which is consists of: (1) protonation of –OH, –COOH, or $–SO_3H$ on the surface of M (Fe) and GO (graphene oxide) and then adsorption of $HCrO_4^-$ by electrostatic attraction; (2) reduction of Cr(VI) on the solid surface to Cr(III) with the assistance of acidic groups, vast π system and phenolic groups on SMGO. These are summarized in Scheme 2.

3.4 Thermodynamic study

Thermodynamic parameters Gibbs free energy (ΔG), standard change in enthalpy (ΔH), and standard change in entropy (ΔS) were explored at 293, 313, and 333 K. eqn (6) and 7 shown below were used.

$$\ln\left(\frac{q_e}{C_e}\right) = -\frac{\Delta H}{RT} + \frac{\Delta S}{R} \quad (6)$$

$$\Delta G = -T\Delta S + \Delta H \quad (7)$$

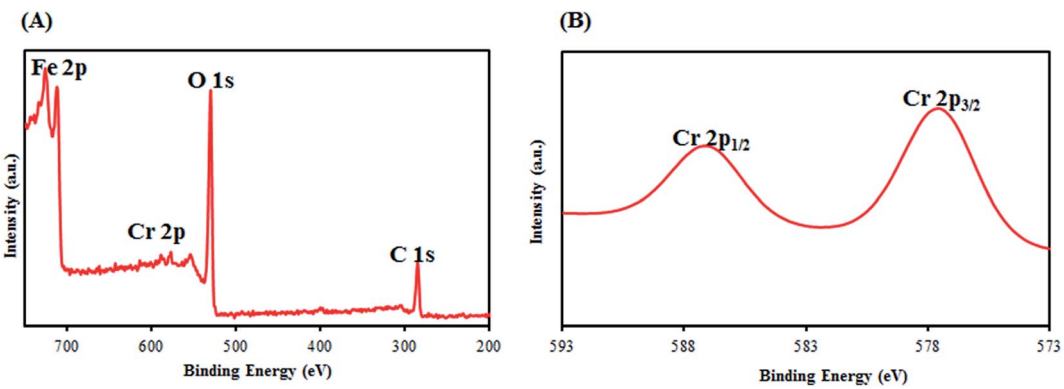

Fig. 10 X-ray photoelectron spectroscopy (XPS) spectra: (A) wide scan, (B) Cr2p spectra of SMGO after adsorption process.

$$\text{GO-M-SO}_3\text{H (s)} + \text{H}^+\text{(aq)} + \text{HCrO}_4^-\text{(aq)} \longrightarrow [\text{GO-M-SO}_3\text{H}_2^+][\text{HCrO}_4^-]\ \text{(s)} \quad (1)$$

$$\text{GO-SO}_3\text{H (s)} + \text{H}^+\text{(aq)} + \text{HCrO}_4^-\text{(aq)} \longrightarrow [\text{GO-SO}_3\text{H}_2^+][\text{HCrO}_4^-]\ \text{(s)} \quad (2)$$

$$\text{GO-COOH (s)} + \text{H}^+\text{(aq)} + \text{HCrO}_4^-\text{(aq)} \longrightarrow [\text{GO-COOH}_2^+][\text{HCrO}_4^-]\ \text{(s)} \quad (3)$$

$$\left\{\begin{array}{ll}[\text{GO-M-SO}_3\text{H}_2^+][\text{HCrO}_4^-] & \text{(s)}\\ [\text{GO-SO}_3\text{H}_2^+][\text{HCrO}_4^-] & \text{(s)}\\ [\text{GO-COOH}_2^+][\text{HCrO}_4^-] & \text{(s)}\end{array}\right. \xrightarrow{3e^-} \text{Cr}^{3+} + \text{H}_2\text{O} \quad (4)$$

Scheme 2

Where T (in K) is the temperature of the system in Kelvin and R (8.3145 J mol^{-1} K^{-1}) is the ideal gas constant.

The values for $-\Delta H/R$ and $\Delta S/R$, which are equal to the slope and intercept of the straight line in Fig. 11, were obtained by plotting $\ln(q_e/C_e)$ against $1/T$. The corresponding thermodynamic parameters were also calculated and listed in Table 6. The positive ΔH value suggest that the adsorption process is endothermic, which is in accordance with the increasing adsorption as the temperature increases. The main cause of endothermic process is this fact that Cr(VI) is well-dissolved in water and hydration cover has to be broken down before its adsorption on SMGO hybrids. This dehydration process needs high temperature. It can be inferred that the endothermicity of desolvation process is higher than the enthalpy of adsorption to a considerable extent. With the increase of temperature the value of ΔG becomes more negative, which is a good sign of a spontaneous process. At high temperature, chromium is desolvated easily which made its adsorption more favorable. The positive value of ΔS indicates the fact that the degree of freedom increases at the solid-phase interface during the adsorption of Cr(VI) on SMGO hybrid. When adsorption occurs, Cr(VI) ions in solution which were surrounded by a highly ordered hydration layer come into close interaction with the hydration cover of SMGO and the order of water molecules are disturbed, resulting in the increased freedom of the system. However, the adsorption of Cr(VI) ions on SMGO may decrease the degree of freedom of system, but the entropy increase of water molecules surpasses the entropy decrease of Cr(VI) ions. It can be concluded that the adsorption of Cr(VI) on SMGO is an endothermic and spontaneous process. The thermodynamic parameters are related not only to the properties of sorbate but also to the properties of solid particles.[42]

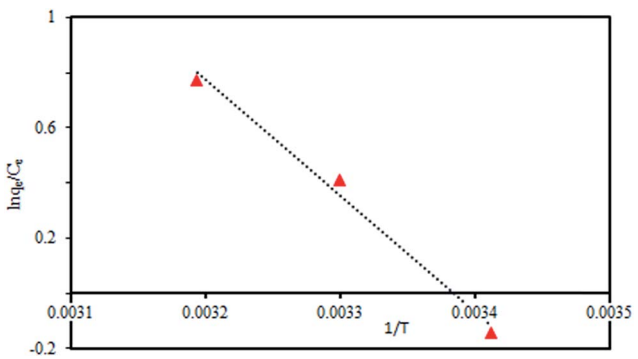

Fig. 11 Plot of $\ln(q_e/C_e)$ *versus* $1/T$ for the adsorption of Cr(VI) on SMGO. Mass of SMGO = 0.5 g L^{-1}, initial concentration of Cr(VI) = 100 mg L^{-1}, contact time = 60 min, pH = 3, volume of Cr(VI) = 40 mL.

Table 6 Thermodynamic parameters for Cr(VI) adsorption on SMGO at different temperatures

T (K)	ΔH (kJ mol^{-1})	ΔS (J mol^{-1} K^{-1})	ΔG (kJ mol^{-1})
293	35.079	118.7144	2.976
303	—	—	−0.891
313	—	—	−2.779

3.5 The reusability of GO/Fe_3O_4/SO_3H hybrids

The stability and potential regeneration of SMGO were studied. The measured zeta potential of SMGO hybrid in pH = 3 (∼+34) confirms that these colloids are positively charged and therefore, they are very stable. As it was explained earlier, chromate ion ($HCrO_4^-$) could be adsorbed onto the positively charged SMGO surface through an electrostatic interaction. This clearly causes the surface of SMGO be saturated (occupied) and for reusing of adsorbent, it is necessary to wash out the adsorbed material from surface. Washing the used adsorbent with NaOH solution (pH ∼ 10) leads to the replacement of chromate with OH^- ion at the surface of SMGO. This is shown in Fig. 9C which confirms the desorption process of chromate (as CrO_4^{2-} in pH > 6) into the solution. On the other hand, in this pH (basic) the functional groups of surface of SMGO are as $-SO_3^-$, $-O^-$, $-COO^-$ which are not suitable for reuse in adsorption of negatively

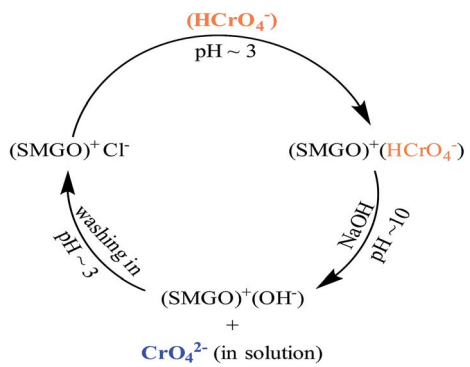

Scheme 3

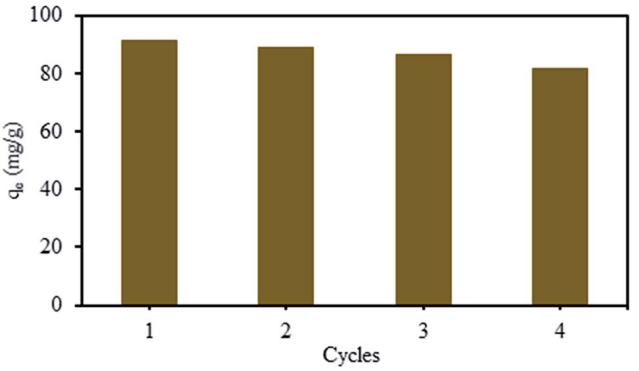

Fig. 12 Recycling of SMGO for the adsorption of Cr(VI). The concentration of SMGO was 1.0 mg L^{-1}, initial concentration of Cr(VI) = 100 mg L^{-1}, temperature = 298 K, contact time = 60 min, pH = 3.

charged $HCrO_4^-$. Therefore, an acid treatment process (stirring of recovered SMGO in a solution pH ~ 3) is needed to regenerate positive surface before the next run of adsorption (Scheme 3).

Several adsorption–desorption cycles were carried out and the recovery analyses were performed. The adsorption capacities of SMGO after recycling for Cr(VI) is illustrated in Fig. 12, which shows that only a slight loss in adsorption capacity can be seen after four consecutive cycles of adsorption–desorption. The results indicate that SMGO, as a good adsorbent, can be recycled in the removal of Cr(VI) ion from aqueous solution.

4. Conclusions

Magnetic hybrid consisting of GO, Fe_3O_4, and sulphonic acid moiety (SMGO) were successfully prepared. The SMGO hybrid exhibited good water-dispersity, simple and rapid separation, high adsorption capacity for chromium removal in water due to the high surface area and the abundant of functional groups of adsorbent. The pseudo-second order kinetic model best describes the adsorption behavior of the Cr(VI) on SMGO. These materials exhibited remarkable adsorption capacity at relatively lower pH value solutions. Langmuir adsorption isotherm gave a good fit to the adsorption data with an adsorption capacity of 222.22 mg g^{-1}. The adsorbed chromium could be effectively washed out from the sorbent into the solution using 2 M NaOH (2 mL) and the surface adsorption sites of SMGO reactivated by HCl (pH ~ 3) washing process. This ensures the process to be economical and eco-friendly. The reusability of SMGO hybrid indicated that it could have great potential applications in removing metal ions from polluted water. Thermodynamic studies revealed that adsorption process is exothermic and spontaneous.

Acknowledgements

The authors are grateful to Razi University and Melbourne University for their financial support for accomplishment of the work and providing necessary facilities. G. Abdi is also thankful to the Iran Nanotechnology Initiative Council (INIC) for their partial support on this project.

References

1 G. Liu, S. Gui, H. Zhou, F. Zeng, Y. Zhou and H. Ye, *Dalton Trans.*, 2014, **43**, 6977–6980.
2 Q. Liu, Q. Liu, W. Ma, W. Liu, X. Cai and J. Yao, *Colloids Surf., A*, 2016, **511**, 8–16.
3 M. Sahranavard, A. Ahmadpour and M. R. Doosti, *Eur. J. Sci. Res.*, 2011, **58**(3), 392–400.
4 G. Bayramoğlu and M. Y. Arıca, *Sep. Purif. Technol.*, 2005, **45**, 192–199.
5 H. Faghihian and M. Rasekh, *Iran. J. Chem. Chem. Eng.*, 2014, **33**(1), 45–51.
6 Y. Zeng, H. Woo, G. Lee and J. Park, *Desalination*, 2010, **257**, 102–109.
7 N. Sankararamakrishnan, A. Dixit, L. Iyengar and R. Sanghi, *Bioresour. Technol.*, 2006, **97**, 2377–2382.
8 M. Tan, X. Liu, W. Li and H. Li, *J. Chem. Eng. Data*, 2015, **60**(5), 1469–1475.
9 M. Yusuf, M. A. Khan, M. Otero, E. C. Abdullah, M. Hosomi, A. Terada and S. Riya, *J. Colloid Interface Sci.*, 2017, **493**, 51–61.
10 F. Zhang, Y. Song, S. Song, R. Zhang and W. Hou, *ACS Appl. Mater. Interfaces*, 2015, **7**, 7251–7263.
11 M. Liu, C. Chen, J. Hu, X. Wu and X. Wang, *J. Phys. Chem. C*, 2011, **115**, 25234–25240.
12 L. Cui, Y. Wang, L. Gao, L. Hu, L. Yan, Q. Wei and B. Du, *Chem. Eng. J.*, 2015, **281**, 1–10.
13 H. Wang, X. Yuan, Y. Wu, H. Huang, G. Zeng, Y. Liu, X. Wang, N. Lin and Y. Qi, *Appl. Surf. Sci.*, 2013, **279**, 432–440.
14 H. Wang, X. Yuan, G. Zeng, Y. Wu, Y. Liu, Q. Jiang and S. Gu, *Adv. Colloid Interface Sci.*, 2015, **221**, 41–59.
15 H. Wang, X. Yuan, Y. Wu, X. Chen, L. Leng, H. Wang, H. Li and G. Zeng, *Chem. Eng. J.*, 2015, **262**, 597–606.
16 X. Yang, X. Zhang, Y. Ma, Y. Huang, Y. Wang and Y. Chen, *J. Mater. Chem.*, 2009, **19**, 2710–2714.
17 X. Yang, C. Chen, J. Li, G. Zhao, X. Ren and X. Wang, *RSC Adv.*, 2012, **2**, 8821–8826.
18 H. Wang, X. Yuan, Y. Wu, H. Huang, X. Peng, G. Zeng, H. Zhong, J. Liang and M. Ren, *Adv. Colloid Interface Sci.*, 2013, **195**, 19–40.
19 W. S. Hummers Jr and R. E. Offeman, *J. Am. Chem. Soc.*, 1958, **80**, 1339.
20 J. Basett, R. Denney, G. Jerrery and J. Mendham, *Vogel's Text Book of Quantitative Inorganic Analysis*, Longman Group, England, 1986, pp. 1–6.
21 G. Liu, S. Gui, H. Zhou, F. Zeng, Y. Zhou and H. Ye, *Dalton Trans.*, 2014, **43**, 6977–6980.
22 V. Chandra, J. Park, Y. Chun, J. W. Lee, I.-C. Hwang and K. S. Kim, *ACS Nano*, 2010, **4**, 3979–3986.
23 S. M. Chackalackal and F. E. Stafford, *J. Am. Chem. Soc.*, 1966, **88**, 4815–4819.
24 X.-j. Hu, Y.-g. Liu, H. Wang, A.-w. Chen, G.-m. Zeng, S.-m. Liu, Y.-m. Guo, X. Hu, T.-t. Li and Y.-q. Wang, *Sep. Purif. Technol.*, 2013, **108**, 189–195.
25 K. Urbas, M. Aleksandrzak, M. Jedrzejczak, M. Jedrzejczak, R. Rakoczy, X. Chen and E. Mijowska, *Nanoscale Res. Lett.*, 2014, **9**, 1–12.

26 A. Alizadeh, M. M. Khodaei, M. Beygzadeh, D. Kordestani and M. Feyzi, *Bull. Korean Chem. Soc.*, 2012, **33**, 2546–2552.
27 A. Jorio, M. S. Dresselhaus, R. Saito and G. Dresselhaus, *Raman spectroscopy in graphene related systems*, John Wiley & Sons, 2011.
28 R. Voggu, B. Das, C. S. Rout and C. Rao, *J. Phys.: Condens. Matter*, 2008, **20**, 472204.
29 A. C. Ferrari and J. Robertson, *Phys. Rev. B: Condens. Matter Mater. Phys.*, 2000, **61**, 14095.
30 H. Iida, K. Takayanagi, T. Nakanishi and T. Osaka, *J. Colloid Interface Sci.*, 2007, **314**, 274–280.
31 A. Özcan, E. M. Öncü and A. S. Özcan, *Colloids Surf., A*, 2006, **277**, 90–97.
32 H. B. de Oliveira and F. Wypych, *J. Solid State Chem.*, 2016, **243**, 136–145.
33 L. Wei, H. Zhang, Y. Dong, W. Song, X. Liu and Z. Zhao, *RSC Adv.*, 2016, **6**, 71375–71383.
34 P. Guzel, Y. A. Aydın and N. Deveci Aksoy, *Int. J. Environ. Sci. Technol.*, 2016, **13**, 1277–1288.
35 N. Sahiner, S. Demirci, M. Sahiner and S. Yilmaz, *J. Appl. Polym. Sci.*, 2016, **133**(20), 43438.
36 L. Li, C. Luo, X. Li, H. Duan and X. Wang, *Int. J. Biol. Macromol.*, 2014, **66**, 172–178.
37 D. Park, S.-R. Lim, Y.-S. Yun and J. M. Park, *Bioresour. Technol.*, 2008, **99**, 8810–8818.
38 Y. Wang, D. Liu, J. Lu and J. Huang, *Colloids Surf., A*, 2015, **481**, 133–142.
39 T. Karthikeyan, S. Rajgopal and L. R. Miranda, *J. Hazard. Mater.*, 2005, **124**, 192–199.
40 H. Wang, X. Yuan, Y. Wu, G. Zeng, X. Chen, L. Leng, Z. Wu, L. Jiang and H. Li, *J. Hazard. Mater.*, 2015, **286**, 187–194.
41 B. Stanton, L. Zhu and C. Atwood, *Experiments in General Chemistry: Featuring MeasureNet*, Cengage Learning, 2009.
42 D. Shao, Q. Fan, J. Li, Z. Niu, W. Wu, Y. Chen and X. Wang, *Microporous Mesoporous Mater.*, 2009, **123**, 1–9.